I&EC research
Industrial & Engineering Chemistry Research

pubs.acs.org/IECR
Article

Enhancing Reactive Microemulsion Processes: Dynamic Optimization and Cyclic Semibatch Operation for the Reductive Amination of Undecanal in a Mini-Plant

Karsten Duch,* Volodymyr Kozachynskyi, Karsten H. G. Rätze, Markus Illner, Kai Sundmacher, and Jens-Uwe Repke

Cite This: *Ind. Eng. Chem. Res.* 2025, 64, 520−534

ABSTRACT: Achieving the maximum production rate of a chemical component in a process requires an optimal process design and operating strategy. One possible approach toward this goal is the elementary process function (EPF) optimization where the optimal temperature, pressure, and mass flow profiles for a Lagrangian fluid element are determined. In the current study, the EPF methodology is applied to the reductive amination of long-chain aldehydes in microemulsion systems (MES) to maximize the reaction performance. These solvent systems are a multiphase green chemistry approach to combine highly selective homogeneous catalysis with excellent catalyst retention using a water phase. For the reductive amination in MES, a cyclic semibatch operation is selected as the best approximation of the optimal EPF trajectories. This new process concept is implemented in a modular mini-plant, and successful validation of the optimization results is achieved for 19 consecutive semibatch reactions during a 125 h mini-plant campaign. The yield (43.8 ± 3.3) %, selectivity (64.3 ± 5.4) %, and conversion (68.0 ± 3.4) % are higher than those achieved in a previous mini-plant operation using a CSTR. Especially, the strong increase in selectivity, achieved through suppression of side product formation, proves that the EPF calculation can lead to a better process design and operating strategy. 99.1% of the catalyst entering the settler is recycled to the reactor, and the reaction performance remains constant for 125 h without requiring additional catalyst. This excellent catalyst retention and long-term stability support the results of previous studies, which outline the large potential of microemulsion systems as reaction media for homogeneous catalysis and their readiness for process implementations.

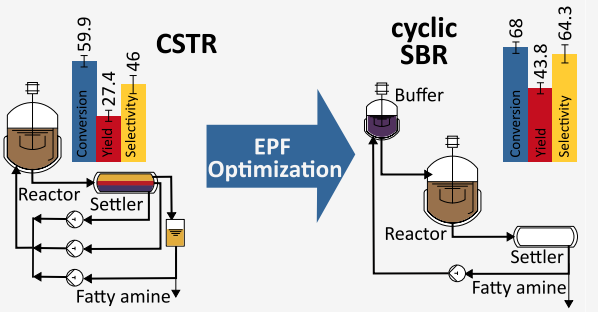

1. INTRODUCTION

Microemulsion systems (MES) offer a way to combine atom-efficient homogeneous catalysis with excellent catalyst retention, which presents a very interesting option for new sustainable industrial processes.[1−4] In MES, water-soluble ligands are attached to the homogeneous catalyst to enable the separation of a polar, catalyst-containing water phase from a nonpolar product phase after the reaction.[5] To increase mass transfer between the polar and nonpolar phase, surfactants are added to microemulsion systems.[6,7] Liquid multiphase reaction systems can be applied for the selective conversion of long-chain hydrocarbons. This is especially interesting for the usage of sustainable organic feedstocks that usually have long carbon chain-lengths such as oleo compounds (e.g fatty acids).[8]

In previous investigations, the hydroformylation[9,10] and the reductive amination (RA)[11] of (>C11) hydrocarbons in MES have already been successfully operated continuously in a mini-plant for over 200 h. For both reactions, good reaction performance and excellent catalyst retention were demonstrated. The current work focuses on the RA as the second step in the hydroaminomethylation (HAM) tandem reaction, in which the hydroformulation and RA can be combined.

In the current investigation, two goals are pursued. First, an optimal process concept and operating strategy for the RA in MES is derived through a dynamic elementary process function (EPF) optimization. Second, the new process concept is implemented in a mini-plant, and the optimization results are verified and compared to previous RA MES investigations.

The RA of undecanal to the fatty amine diethylundecylamine is an example of a complex reaction network for the production of fine chemicals. During the reaction, undecanal is converted in an equilibrium reaction with diethylamine (DEA) to an enamine intermediate, which is catalytically hydrated to a

Received: July 12, 2024
Revised: November 13, 2024
Accepted: November 15, 2024
Published: December 20, 2024

https://doi.org/10.1021/acs.iecr.4c02607
Ind. Eng. Chem. Res. 2025, 64, 520−534

fatty amine in a subsequent reaction.[12,13] The enamine intermediate also reacts with undecanal in an undesired side reaction toward aldols.[12,13] The aim of the EPF optimization is to find an optimal process design and operating strategy with which a maximum fatty amine yield of the RA can be achieved. This optimization is necessary because the aldol side reaction could not be sufficiently suppressed in continuous operation, resulting in unfavorable selectivity and yield.[11]

Elementary process functions are a model-based methodology to determine optimal process setups and operating strategies for a given reaction.[14,15] Instead of optimizing a combination of process units, the design space is expanded and optimal control profiles for a Lagrangian fluid element are determined. The EPF optimization methodology is chosen for the current investigation because it is able to represent the large design space and complex interactions in microemulsion systems. It has also been successfully applied to and verified in reactive multiphase systems.[16−19]

To derive a continuous process design from the optimal EPF trajectories, flux profile analysis (FPA) was developed, where the trajectories are analyzed and divided into sections, each corresponding to an ideal reactor unit.[20] A combination of these reactor units enables the design of a reactor network without limiting the design space to a set of predefined unit operations.[20] The FPA has been successfully implemented for the hydroformylation in thermomorphic solvent systems (TMS)[17,18] and was experimentally verified.[19] TMS are an alternative liquid two-phase approach that enable catalyst recycling in a polar phase, where cosolvents are used instead of surfactants to ensure miscibility of nonpolar and polar components.[21−23] In the current investigation, EPF optimization and FPA are applied for the first time to reactive MES.

As part of the investigation, a kinetic model for the RA in MES is set up and parameters are estimated based on experimental results.[13] The model is then used in an EPF optimization to determine the optimal reaction trajectory and operating conditions. A subsequent FPA reveals that the optimal trajectory can best be approximated by a semibatch reactor (SBR). Afterward, an optimization problem with fewer degrees of freedom and additional mini-plant constraints is formulated to maximize the performance of the SBR implementation in a real mini-plant online. A new process design in combination with phase separation and cyclic operation is derived for the SBR and implemented in a modified modular mini-plant. In addition, accurate surfactant tracking and dosing are introduced for the first time in a mini-plant operation to increase the controllability of the reaction and separation performance. Finally, the EPF predictions are verified with experimental results in a 125 h campaign. The results are furthermore compared to other operating modes to assess the improvement achieved with the EPF methodology.

2. THEORETICAL BACKGROUND

2.1. Microemulsion Systems as Reaction Media. MES can be used as a multiphase reaction medium to achieve good reaction performance and excellent separation of the homogeneous catalyst from the formed product after the reaction.[24,25] The catalyst is attached to water-soluble ligands to separate it from the nonpolar educt and product in a polar water phase. A surfactant is required in MES to increase the mass transfer between the two phases with opposing polarities during the reaction. The separation of catalyst and product is achieved through temperature-controlled liquid phase separation, where the catalyst and water-soluble ligands are retained in the polar water phase.

In addition to temperature, phase separation behavior is also influenced by the concentration of each component in the mixture. Since thermodynamic models for the description of phase separation involving surfactants are not yet available, an experimental investigation is required[26] as previously conducted for the RA.[11]

As Figure 1 shows, microemulsions exhibit distinct liquid−liquid phase separation states[27,28] which can be exploited for a reaction medium with catalyst separation.[24]

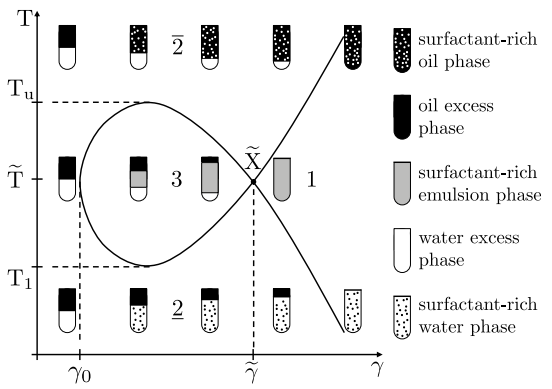

Figure 1. Kahlweit fish-diagram, redrawn from Sottmann and Stubenrauch.[28] Copyright 2009 Wiley.

Two characteristic surfactant concentrations mark the boundaries of the region in which MES can be used for reaction and separation. The lower bound is the critical micelle concentration (cmc) γ_0, at which the phase interface is saturated with surfactant molecules and micelle surfactant agglomerates form. Below the cmc (γ_0), the polar and nonpolar components separate into two liquid phases, and the phase-interface is too small to achieve good reaction rates.[29] The second characteristic concentration is $\tilde{\gamma}$. If the concentration of surfactant increases beyond this point, a stable emulsion is formed that does not separate into multiple phases[27,28] and can, hence, not be used for catalyst separation. The region of interest for reactive MES is between these two critical surfactant concentrations, where, depending on temperature, three relevant phase configurations occur. At low temperatures, the first separation state of interest is the $\underline{2}$-region, where a nonpolar oil phase with low surfactant and catalyst content, and a polar water excess phase with high catalyst and surfactant content are formed. In the water phase, micelle-enclosed oil droplets are also present. In the 3-phase region at higher temperatures, a water and oil phase form, each with low surfactant content (only cmc[30]), along with a third emulsion phase that contains the bulk of the surfactant. This phase state is the most interesting for continuous operation, as it has the shortest separation time.[31] The third separation state that can be achieved at high temperatures is the $\bar{2}$-region, where an excess water phase and an oil phase with micelle-enclosed water droplets form. Due to the enclosed catalyst in the water in oil micelles, the $\bar{2}$-region is undesirable for catalyst recovery.

The main reason for operating the continuous phase separation in the three-phase region is the short separation time. However, even at short separation times in the two-phase region, as observed for the RA in our previous separation investigation,[11] this region is still not suitable for continuous

https://doi.org/10.1021/acs.iecr.4c02607
Ind. Eng. Chem. Res. 2025, 64, 520−534

separation. In continuous three-phase separation, a visual feedback of the separation state in the settler is vital for a stable process control, as it is used to monitor the influences of a concentration shift on the phase-separation.[10,30] The change in separation state can be observed through clouding of either the oil or the water phase, and the settler temperature can be adjusted to stay within the three-phase region. For the two-phase separation, there is no visual feedback of a changing separation state in case of a concentration shift, which may lead to unexpected incomplete separation in the settler and a halt of the continuous operation. In discontinuous operation, however, 2-separation is easy to maintain and the lower surfactant content in the oil phase at lower temperatures is desirable. The 2-separation is thus also investigated on a mini-plant scale in the current contribution.

2.2. Reductive Amination in Microemulsion Systems. The first step in the main reaction pathway of the RA is an equilibrium reaction between diethylamine (DEA) and undecanal toward the enamine intermediate (eq 1a), as shown in the reaction network in Figure 2. In a subsequent

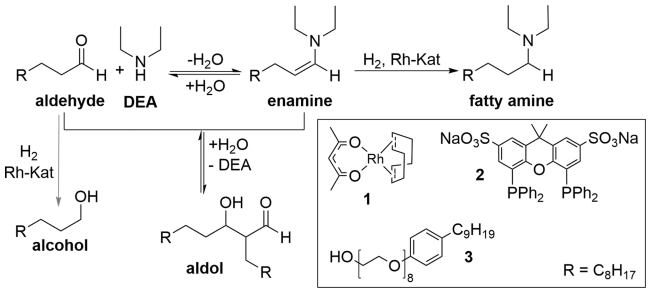

Figure 2. Reaction network of the reductive amination of undecanal to diethylundecylamine in microemulsions, proposed by Kirschtowski et al.[12] and adapted by Weber et al.[13] (catalyst 1 = Rh(acac)(COD), ligand 2 = SulfoXantphos, surfactant 3 = Marlophen NP8). Reproduced from ref 13. Available under a CC-BY 4.0 license. Copyright Weber et al.

reaction, the enamine is catalytically hydrated toward the desired fatty amine, diethylundecylamine (DEUA) (eq 1b).[12,13] The reaction network also includes two undesired side reactions. The first is the catalytic hydration of undecanal to undecanol (eq 1c), which can be fully suppressed by adding CO to the gas phase.[13] The CO does not take part in the reaction but acts as a ligand and shifts the catalyst equilibrium toward a state which is only active in the desired fatty amine catalysis.[13] The second side reaction is an equilibrium reaction between the undecanal substrate and the enamine intermediate toward aldols (eq 1d). The reaction is strongly dependent on the enamine and aldehyde concentrations. Dodecane is hence introduced as a cosolvent to dilute the aldehyde concentration and, thus, limit the side reaction.[13] As our previous continuous mini-plant investigation[11] showed, the obtained selectivity and yield toward the fatty amine are still not fully satisfactory (S: (46.0 ± 5.3) % Y: (27.4 ± 3.3) %[11]), and further investigations to increase the selectivity and yield are required.

2.3. Fundamentals of Elementary Process Functions and Flux Profile Analysis. Approaches for reactor-network design can be divided into three categories: heuristics, attainable region (AR) approaches, and optimization-based approaches.[15,32] Heuristics rely on experience or large amounts of data without requiring a model. Their prediction capabilities, however, are very limited and they can not be applied for the design of new complex reaction systems.[15] The attainable region (AR) design methodology maps out the complete design space for an arbitrary process application but without identifying an optimal path within this region, as the EPF methodology does.[15] Along with superstructure optimization, the EPF methodology falls into the category of optimization-based approaches.[15,20] In superstructure optimization the design space is restricted to preselected process units that require a full model for each subunit, and integer decision variables to select between units result in an MINLP, requiring advanced solution approaches.[33] The superstructure approach for process design under the inclusion of model uncertainties was demonstrated for the hydroformylation of decene in a multiphase reaction system.[34] In addition to superstructure optimization, dynamic Programming can also be used for process synthesis. Due to a higher level of abstraction, this leads, in the case of the EPF methodology, to an NLP and, therefore, a reduction in problem complexity.[15] An extended comparison of EPF to other process design and optimization approaches can be found in literature.[15,20,32] The EPF methodology provides dynamic trajectories for decision variables that can also be used in advanced process control schemes.[32] Other approaches for optimal control of MES processes such as dynamic real-time optimization with state estimation[35] to reduce the mismatch between measurements and an uncertain process model have been investigated for the hydroformylation.[36,37] For the design and operation of an RA process in MES, the EPF methodology is selected to achieve an optimal process design in a large unrestricted design space with a reduced model complexity.

In an EPF investigation, the process of interest is conceptualized as a Lagrangian fluid element traveling through state space.[20] The path of the fluid element is constrained by the kinetics of the reaction. However, by optimally adjusting fluxes (e.g., heat- and mass-fluxes), the path as well as the final destination in state space can be influenced by a predefined objective function. Consequently, the EPF methodology yields optimal control profiles for temperature, pressure, etc. which can be successively refined with respect to additional physical, technical, economic, or environmental constraints to approximate feasible real-world reactor networks.[14,15] The optimal reaction path is derived from a dynamic optimization problem in which the reaction in the fluid element and the mass and energy fluxes into the element are described by equations, as shown in eq 10. The results of the optimization for a multiphase system are e.g. temperature and pressure profiles of the fluid element during the reaction time, as well as external mass flows of reactants into the element.[20]

To find a feasible reactor concept that can approximate the resulting profiles, the FPA is applied as an extension of the EPF.[17,20] The FPA can be divided into three steps. The first step is a dynamic optimization, as in the EPF methodology, with the extension of introducing virtual storage tanks for all reacting components (educts and products) from which the components can be fed into the fluid element. The possibility of dosing product components enables the introduction of back-mixing characteristics and product recycling. During the reaction time, the educts are fully supplied to the fluid element with dynamic adjustments of the feed rate by the optimizer. In case the optimizer decides to feed a product component to the fluid element, the same amount of product will be returned to the product tank at the end of the reaction time so as not to violate the overall mass balance. The supply of products during

https://doi.org/10.1021/acs.iecr.4c02607
Ind. Eng. Chem. Res. 2025, 64, 520−534

the reaction is an indication that back mixing is a desirable characteristic when selecting a reactor type for the reaction. Components such as the catalyst and surfactant, which do not directly take part in the reaction or are not consumed, are initially supplied in the fluid element. In addition to substance feed profiles, the EPF calculation also yields dynamic temperature and pressure profiles for the fluid element. In the second step of the FPA, the resulting profiles are divided into characteristic sections (e.g., constant pressure or temperature). In the third step, reactor types are selected that can best approximate the behavior of the profile sections. A lookup table to match the flux profiles to either a plug flow reactor (PFR) distributed side-stream reactor (DSR) or a continuously stirred tank reactor (CSTR) can be found e.g. in Kaiser et al.[20]

3. PROCESS SYNTHESIS FOR THE REDUCTIVE AMINATION IN MICROEMULSION SYSTEMS USING ELEMENTARY PROCESS FUNCTIONS

3.1. Kinetic Model Development for the RA in MES.

To perform the EPF optimization/FPA, a kinetic model is required. For the RA in TMS, such a model was developed[12,38] and is adapted here to be used for microemulsion systems following a previously developed procedure.[39] One major difference between the TMS and MES is the presence of large amounts of water in MES, which takes part in the reaction and has a negative influence on the selectivity, as it contributes to higher aldol formation (see Figure 2, eq 1d).[13,38,40] Furthermore, the influence of the surfactant on the reaction also needs to be taken into account. The rate equations r in mol^2 L^{-2} of the reaction network are

$$r_{\mathrm{EQa}} = \mathrm{trig}(T) k_{\mathrm{EQa}}(T)\left(c_{\mathrm{nC11al}} c_{\mathrm{DEA}} - \frac{c_{\mathrm{En}} c_{\mathrm{H_2O}}}{K_{\mathrm{EQa}}}\right) \tag{1a}$$

$$r_{\mathrm{HYDa}} = \mathrm{trig}(T)\psi(c)\mathrm{LM}(c)\gamma(c) k_{\mathrm{HYDa}}(T) c_{\mathrm{En}} c_{\mathrm{H_2}}^{\mathrm{sat}} \tag{1b}$$

$$r_{\mathrm{HYDb}} = \mathrm{trig}(T)\psi(c)\mathrm{LM}(c)\gamma(c) k_{\mathrm{HYDb}}(T) c_{\mathrm{nC11al}} c_{\mathrm{H_2}}^{\mathrm{sat}} \tag{1c}$$

$$r_{\mathrm{EQb}} = \mathrm{trig}(T) k_{\mathrm{EQb}}(T)\left(c_{\mathrm{nC11al}} c_{\mathrm{En}} c_{\mathrm{H_2O}} - \frac{c_{\mathrm{Aldols}} c_{\mathrm{H_2O}}}{K_{\mathrm{EQb}}}\right) \tag{1d}$$

The variables in eq 1a−1d are r_{EQa} as the aldehyde/enamine equilibrium-reaction rate, r_{HYDa} as the rate of enamine hydration, r_{HYDb} the rate of the aldehyde hydration side reaction, r_{EQb} as the aldol side reaction equilibrium, and the component concentrations c_i (see Table 1) in mol L^{-1}. The expressions for the Arrhenius dependence k_j (eq 2a) in all rate equations ($\mathcal{RCT}$) and the equilibrium constant K_k (eq 2b) are

$$k_j = k_{0,j} \exp\left(\frac{-E_{\mathrm{A},j}}{RT}\right), \quad \forall\, j \in \mathcal{RCT} \tag{2a}$$

$$K_k = \exp\left(\frac{-\Delta G_{\mathrm{r},k}}{RT}\right), \quad \forall\, k \in \{\mathrm{EQa},\ \mathrm{EQb}\} \tag{2b}$$

The concentration of hydrogen dissolved in the MES mixture $c_{\mathrm{H_2}}^{\mathrm{sat}}$ is calculated with Henry coefficients according to eq S2b−d and Table S3 in the Supporting Information.

Table 1. Component Indices i for All Species $\mathcal{SPC}$

component	index ($i \in \mathcal{SPC}$)
1-undecanal	nC11al
diethylamine	DEA
1-diethylundecylenamine	enamine
1-diethylundecylamine	amine
1-undecanol	nC11OH
aldol	Aldol
water	H2O
dodecane	nC12an
Rh(acac)(CO)$_2$	cat
sulfo-Xantphos	ligand
marlophen NP8	surf

In eq 1a−1d, four new expressions ($\gamma(c)$, $\psi(c)$, LM(c), trig(T)) are introduced compared to the original rate equations by Kirschtowski et al.[12] The first expression in eq 3

$$\gamma(c) = \exp\left(K_{\gamma}^{\mathrm{opt}}\left(\frac{M_{\mathrm{surf}} c_{\mathrm{surf}}}{\sum_{i\in\mathcal{SPC}} M_i c_i}\right)^2\right) \tag{3}$$

accounts for the surfactant concentration, which affects the reaction rate due to its influence on mass transport between the phases with opposite polarities. Here, M represents the molar mass in g mol^{-1} (see Table S6). γ is calculated in relation to all other nongaseous species $i \in \mathcal{SPC}$ present in the MES mixture.

The expression in eq 4

$$\psi(c) = \frac{c_{\mathrm{cat}}}{1 + K_{\mathrm{cat}} \frac{c_{\mathrm{DEA}}}{c_{\mathrm{H_2O}}}} \tag{4}$$

is an adjustment to incorporate the equilibrium of the catalyst complex, which can be influenced by the DEA concentration c_{DEA} and the resulting pH value.[13] The next expression in eq 5

$$\mathrm{LM}(c) = \exp\left(K_{\mathrm{LM}}^{\mathrm{opt}}\left(\frac{c_{\mathrm{ligand}}}{c_{\mathrm{cat}}} - \mathrm{LM}^{\mathrm{opt}}\right)^2\right) \tag{5}$$

is also connected to the catalyst activity and describes the ligand-to-metal ratio of the catalyst complexes. Lastly, the expression in eq 6

$$\mathrm{trig}(T) = \left(1 - \frac{k_{\mathrm{trig}}}{1 + \exp(p_{\mathrm{trig}}(T - T_{\mathrm{trig}}))}\right) \tag{6}$$

is a trigger function which is included to adapt the model to a disproportionate increase in conversion, which deviates from the Arrhenius dependence (eq 2a) between 100 and 110 °C, as observed in the experiments.[13] $K_{\gamma}^{\mathrm{opt}}$, K_{cat}, $K_{\mathrm{LM}}^{\mathrm{opt}}$, LM$^{\mathrm{opt}}$, k_{trig}, p_{trig}, and T_{trig} were introduced as model parameters that are estimated during parameter estimation. Parameter values for eqs 2a−6 can be found in Tables S1 and S2 of the Supporting Information. The model parameters are fitted to experimental values obtained by Weber et al.[13] using the mopeds python package[41] (example shown in Figure S1 in Supporting Information). The component balances and auxiliary equations of the kinetic model are provided in the Supporting Information (eqs S1 and S2).

https://doi.org/10.1021/acs.iecr.4c02607
Ind. Eng. Chem. Res. 2025, 64, 520−534

3.2. Setup of the EPF Optimization Problem. In this section, an EPF optimization is carried out to assess the maximum potential of the RA process in MES.

As optimization objective for optimal reaction performance, multiple performance indicators such as conversion (X), fatty amine selectivity (S_{Amine}), or fatty amine yield (Y_{Amine}) can be considered:

$$X = \frac{n^{\text{ST}}_{\text{nC11al}}(t = t_0) + n_{\text{nC11al}}(t = t_0) - n_{\text{nC11al}}(t = t_f)}{n^{\text{ST}}_{\text{nC11al}}(t = t_0) + n_{\text{nC11al}}(t = t_0)} \tag{7}$$

$$S_{\text{Amine}} = \left[n_{\text{Amine}}(t = t_f) - \sum_{m \in \{\text{Amine,En}\}} (n_m(t = t_0) + n^{\text{ST}}_m(t = t_0) - n^{\text{ST}}_m(t = t_f)) \right] \Big/ [n^{\text{ST}}_{\text{nC11al}}(t = t_0) + n_{\text{nC11al}}(t = t_0) - n_{\text{nC11al}}(t = t_f)] \tag{8}$$

$$Y_{\text{Amine}} = \left[n_{\text{Amine}}(t = t_f) - \sum_{m \in \{\text{Amine,En}\}} (n_m(t = t_0) + n^{\text{ST}}_m(t = t_0) - n^{\text{ST}}_m(t = t_f)) \right] \Big/ [n_{\text{nC11al}}(t = t_0) + n^{\text{ST}}_{\text{nC11al}}(t = t_0)] \tag{9}$$

The expressions for X, S, and Y each take into account the freedom of the optimizer to dose each of the reacting components into the fluid element from externals storage tanks (n_i^{ST}). The variables in eqs 7–9 are n^{ST} $(t = t_0)$ as the initial molar amount in the external storage tank, n^{ST} $(t = t_f)$ as the amount in the storage tank at the end of the reaction time t_f, and n_{nC11al} $(t = t_0)$ as the initial amount in the reactor. In the expressions for the selectivity and yield, the dosing of amine and the intermediate enamine is also considered. The decision of the optimizer to dose either of these components would artificially increase the selectivity and yield, bypassing the reaction network. Therefore, the initial or dosed amounts of amine and enamine are subtracted.

For the current investigation, the yield is chosen as optimization objective, as it ensures that not only the reaction conversion (X, eq 7) or selectivity (S_{Amine}, eq 8) are maximized ($Y_{\text{Amine}} = S_{\text{Amine}} \cdot X$, eq 9) but the total amount of undecanal converted to fatty amine per batch n_{Amine} $(t = t_f)$. The optimization is set up to find a process configuration that maximizes the reaction performance. Economic parameters are not factored into the objective function as they are still very uncertain at the current development stage.[42]

The dynamic optimization problem used for the EPF flux profile analysis is

$$\min_{n_i(t_0),\, T(t),\, p(t),\, y_{\text{H}_2}(t),\, \xi(t),\, j_i^{\text{ext}}(t)} \; - Y_{\text{Amine}} \tag{10a}$$

s.t.

$$\frac{\text{d}n_i}{\text{d}t} = j_i + j_i^{\text{ext}} + V_{\text{Liq}} \cdot r_i, \quad \forall\, i \in \mathcal{SPC}, \tag{10b}$$

$$\frac{\text{d}n_i^{\text{ST}}}{\text{d}t} = -j_i^{\text{ext}}, \tag{10c}$$

$$j_i = \xi \frac{n_i(t + \Delta t)}{\Delta t} \quad \text{Note: Discretized,} \tag{10d}$$

Kinetic model: (eqs 1a–2b) + (eqs S1 – S2),

$$n_i^{\max} = n_i(t_0) + n_i^{\text{ST}}(t_0), \tag{10e}$$

$$\phi_{\text{cat}} = \frac{n_{\text{cat}}(t_0) + n^{\text{ST}}_{\text{cat}}(t_0) - n^{\text{ST}}_{\text{cat}}(t_f)}{(n_{\text{sub}}(t_0) + n^{\text{ST}}_{\text{sub}}(t_0) - n^{\text{ST}}_{\text{sub}}(t_f))}, \tag{10f}$$

$$\phi_{\text{ligand}} = \frac{n_{\text{ligand}}(t_0) + n^{\text{ST}}_{\text{ligand}}(t_0) - n^{\text{ST}}_{\text{ligand}}(t_f)}{(n_{\text{cat}}(t_0) + n^{\text{ST}}_{\text{cat}}(t_0) - n^{\text{ST}}_{\text{cat}}(t_f))}, \tag{10g}$$

$$\phi_{\text{oil}(t)} = \frac{\sum_{i \in \mathcal{SPC} \setminus \{\text{H}_2\text{O}\}} m_i}{m_{\text{H}_2\text{O}}}, \tag{10h}$$

$$\phi_{\text{surf}}(t) = \frac{m_{\text{surf}}}{\sum_{i \in \mathcal{SPC}} m_i}, \tag{10i}$$

$$\phi_{\text{sub}}(t) = \frac{n_{\text{nC11al}}}{n_{\text{DEA}}}, \tag{10j}$$

Table 2, Table 3,

$$0 = n^{\text{ST}}_{\text{sub}}(t = t_f), \tag{10k}$$

$$0 = V_{\text{Liq}}(t = t_f) - V_{\text{target}}, \tag{10l}$$

$$X \geq 0.8. \tag{10m}$$

The decision variables for the optimization are the initial amounts of each species $i \in \mathcal{SPC}$ (Table 1) in the fluid element $n_i(t_0)$, as well as the temperature $T(t)$, system pressure $p(t)$, the axial dispersion ξ along a finite element, the molar fraction of hydrogen in the gas phase y_{H_2}, and the external component feed streams $j_i^{\text{ext}}(t)$ at any point during the reaction time t_f.

Table 2. Parameters for the Reductive Amination in an MES

parameter	description	value	unit
t_f	reaction time	480.000000	min
ϕ_{cat}	catalyst concentration	0.0000687	mol mol^{-1}
ϕ_{lig}	ligand to metal ratio	4.000000	mol mol^{-1}
ϕ_{oil}	oil fraction	0.500000	g g^{-1}
ϕ_{surf}	surfactant concentration	0.080000	g g^{-1}
ϕ_{sub}	educt ratio	1	mol mol^{-1}
V_{target}	normalization volume	1	L

The optimization is subject to the component mass balances (eq 10b) and the reaction kinetics as defined in eqs 1a–2b and the Supporting Information (eqs S1 and S2). The component

Table 3. Decision Variable Bounds for the EPF Optimization of the RA

decision var.	description	L.b.	U.b.	unit
j_i^{ext}	dosing stream	0		mol h^{-1}
T	temperature	358.15	388.15	K
p	pressure	10.0	29.0	bar
y_{H2}	hydrogen fraction	0.0	1.0	mol mol^{-1}
dT/dt	temperature change rate	$-\infty$	∞	K min^{-1}
dp/dt	pressure change rate	$-\infty$	∞	bar min^{-1}
dy_{H_2}/dt	hydrogen frac. change rate	$-\infty$	∞	1/min
ξ	back-mixing parameter	0.0	1.0	

https://doi.org/10.1021/acs.iecr.4c02607
Ind. Eng. Chem. Res. 2025, 64, 520–534

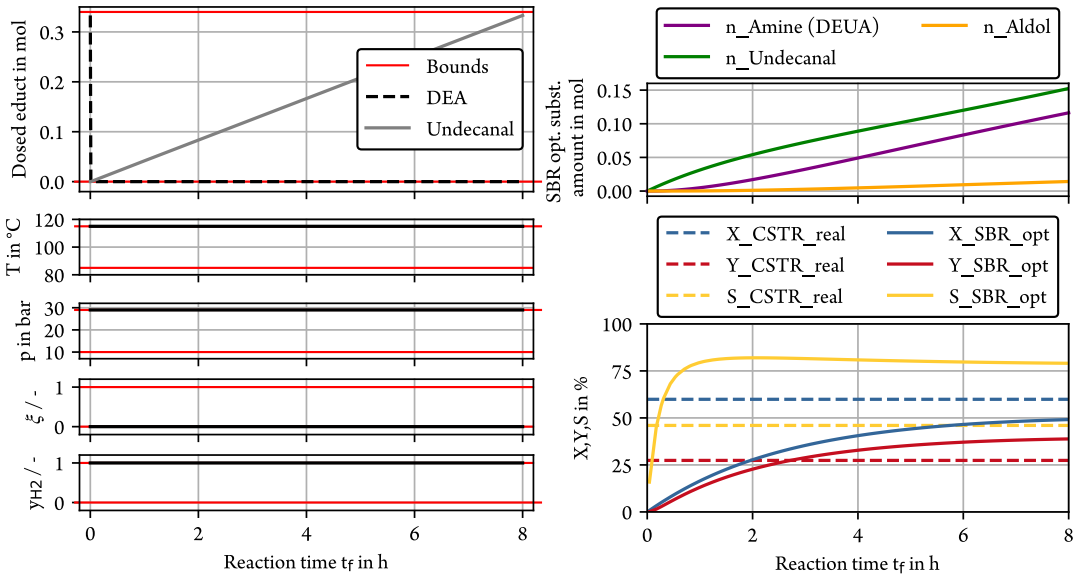

Figure 3. Results of the EPF optimization in eq 10. On the left: Optimal EPF decision variables $n_i(t_0)$, $T(t)$, $p(t)$, $\xi(t)$, $y_{H_2}(t)$, $j_i^{ext}(t)$ for the RA in MES with a reaction time t_f = 8 h. On the right: Molar holdup trajectories of the main reacting components and resulting optimized conversion X, yield Y, and selectivity S with a comparison to experimental mini-plant CSTR base-case results from Duch et al.[11]

mass balances include feed streams from the external storage tank j_i^{ext} (eq 10c) and internal streams j_i (eq 10d) that represent discretized back-mixing between the finite elements. The back-mixing characteristic ξ shows if a PFTR (ξ = 0, no back-mixing) or CSTR (ξ = 1, full back-mixing) behavior is more favorable for the reaction. The initial constraint in eq 10e defines how much of a component is present in the system in total at $t = t_0$. With this definition, the optimizer is able to freely adjust if initial provisioning in the fluid element or dosing over time is more favorable. The total amounts of material n_i^{max} for eq 10e are given in Table S6 in the Supporting Information and also fulfill the constraints in eqs 10f−10j. The constraints in eqs 10f−10j define the catalyst concentration ϕ_{cat} (eq 10f), the ligand to catalyst ratio ϕ_{ligand} (eq 10g), the oil fraction ($\alpha = \phi_{oil}(t)$) (eq 10h), the surfactant concentration ($\gamma = \phi_{surf}(t)$) (eq 10i), and the educt ratio $\phi_{sub}(t)$ (eq 10j). The values of these constraints are given in Table 2 along with the batch reaction time t_f of 8 h. The reaction time is chosen as the kinetic model shows the highest reaction activity within this interval. The constraints in Table 2 are chosen in accordance with the optimal values from kinetic experiments,[13] as used in a previous CSTR study.[11] Fixing these parameters allows for an accurate assessment of the achieved improvement with the EPF optimization in comparison to a CSTR operation. The decision variables are constrained by the bounds given in Table 3. The upper bounds for pressure and temperature are set to the upper limit of the experimentally investigated range for the RA.[13] The rates of change for the decision variables $\frac{d}{dt}$ are not limited to determine the maximum potential of the process, even though these rates may be limited in a real process application. Constraint eq 10k states that the external educt storage tanks have to be empty at the end of the reaction to ensure that the complete component holdup specified in eq 10e takes part in the reaction. In eq 10l, target volume V_{target} is defined to constrain the liquid volume V_{Liq} of the fluid element for normalization purposes. Finally, a minimum conversion X of 80% is specified in eq 10m.

The dynamic optimization problem is discretized using Radau collocation with 3 collocation points and 30 finite elements along the reaction time. The resulting nonlinear optimization problem is solved with multiple shooting[43] using IPOPT 3.12.3[44] with the MA27[45] linear solver using default casadi[46] solver settings.

3.3. FPA of the EPF Process-Optimization Results.

The EPF optimization in eq 10 yields profiles for the decision variables $T(t)$, $p(t)$, initial amount $n_i(t_0)$, component dosing streams $j_i^{ext}(t)$, back-mixing coefficient $\xi(t)$, and gas-phase hydrogen fraction $y_{H_2}(t)$, as shown in Figure 3 on the left.

The first plot on the left shows the initially supplied amount of DEA $n_{DEA}(t_0)$ and undecanal $n_{nC11al}(t_0)$, as well as the integral of the dosing streams $j_{DEA}^{ext}(t)$ and $j_{nC11al}^{ext}(t)$. The EPF methodology reveals that the optimal reaction performance can be achieved if all of the DEA is supplied initially and all of the undecanal is dosed over the complete reaction time t_f. This result is plausible when looking at the reaction network in Figure 2, which shows that the aldehyde concentration is the variable with the strongest influence on the unwanted aldol side-product formation. To keep the aldehyde concentration as low as possible, while also fulfilling the constraint of an empty undecanal storage tank at the end of the reaction (eq 10k), the undecanal feed is distributed across the reaction time at a constant minimum rate.

The decision variables for temperature and pressure in Figure 3 are set to the upper bound (29 bar, 115 °C, see Table 3) throughout the reaction time since these conditions are most favorable for a high reaction rate (eq 1a to 2b, eq S2b,c in Supporting Inforation). The molar gas-phase hydrogen fraction $y_{H_2}(t)$ is set to 1 by the optimizer. This result shows that the underlying kinetic model of the EPF does not accurately display the influence of CO on the alcohol side product formation. Experimental results show that the presence of 33% CO can completely suppress the alcohol formation[13] (Figure 2). To improve the prediction power for y_{H_2} as a degree of freedom in future EPF investigations of the RA, further experimental variations of the gas composition and an

https://doi.org/10.1021/acs.iecr.4c02607
Ind. Eng. Chem. Res. 2025, 64, 520−534

adaptation of the kinetic model would be required. The decision variable $\xi(t)$ is at the lower bound (0) throughout the reaction time, in Figure 3, which implies that back-mixing should be avoided to achieve a maximum reaction performance.

On the right in Figure 3, molar holdup trajectories of the main reacting components are simulated for the optimized SBR. The trajectories show that the amount of amine and undecanal in the reactor increase at the same rate. This indicates that the aldehyde accumulates in the reactor at the same rate at which it is converted to the target product, thus avoiding a limitation of the reaction through a too low aldehyde concentration. In addition to the good match between the feed rate and the fatty amine generation rate, the simulated holdup of the aldol side product also stays low throughout the reaction time. Figure 3 also shows a comparison between the optimized conversion X, yield Y, and selectivity S of the SBR compared to experimental results from a mini-plant CSTR operation under similar conditions.[11] The comparison shows that the EPF optimization successfully results in an operation mode that leads to a higher yield and a much higher selectivity than in the reference case.

As described in the theoretical background, the FPA can be employed to analyze the resulting profiles of the EPF optimization and to derive a process design. As the results in Figure 3 show, the ideal reactor for the RA in MES has the following characteristics: no back-mixing (plug flow behavior), enables a constant pressure, temperature, and gas phase composition, and enables continuous dosing of undecanal. Since the temperature and pressure are constant throughout the reaction time and a constant feed rate is proposed by the EPF optimization, the resulting profiles can be realized in a single reactor. As the goal of the FPA is to design a continuous production process, the reactor type best combining the required characteristics is a distributed side-stream reactor (DSR).[17] However, this option is not chosen due to the complexity of homogeneously distributing the synthesis gas[47] and the undecanal feed along the length of a plug flow reactor. This requires a specially designed PFTR with multiple dosing points where very small undecanal flows are accurately dosed.[47] A constant gas-phase composition with continuous dosing and no back mixing can, however, also be achieved in an SBR. The SBR also has the added benefit of a well-proven simple reactor concept which allows a fast transfer of the optimization results to a mini-plant. To enable the incorporation of an SBR into a continuous process, it needs to combined with two buffer tanks and operated cyclically to replace the DSR, as shown for the hydroformylation in TMS.[17−19] The SBR is used to mimic the reaction characteristic of a DSR and the buffer tanks are added to incorporate the SBR in a process with continuous recycle and product streams. The use of an SBR with a gassing stirrer instead of a DSR also avoids difficulties of ensuring a constant gas-phase composition and mixing the gas and liquid phase faced in previous investigations.[47] The SBR approach is, hence, chosen as the ideal solution to realize the optimization profiles in a mini-plant. A cyclic operation of the SBR with short down-times enables an incorporation into a continuous process and ensures a maximum production capacity of the resulting process design. In addition to the optimal reactor, catalyst separation and recycling also need to be included in the new process design and operating strategy (see Section 4.1).

3.4. Adjusted EPF Implementation for the Online Optimization of a Mini-Plant. With eq 10, an EPF optimization is performed to determine the maximum process potential for the RA in MES. In the subsequent FPA, an SBR is determined as the ideal reactor to realize the results of the process optimization. To implement the new reactor concept in an existing mini-plant and to ensure comparability of the experimental results to previous mini-plant investigations while still maximizing the SBR yield, an adapted and simplified form of the EPF optimization in eq 10 is set up. In this implementation, constraints of a real mini-plant are considered and the optimization problem is simplified (the degrees of freedom are reduced) to enable an online optimization for each produced batch. With the simplification, the decision variables ξ and y_{H_2} are fixed and the constraints for X (eq 10m) and V_{target} (eq 10l) are removed. The adjusted EPF formulation is thus:

$$\min_{n_o(t_0),\, T(t),\, p(t),\, j_o^{ext}(t)} \; -Y_{Amine} \quad \forall o \in \{\text{nC11al, DEA}\}$$

$$\text{s.t.}$$

$$\text{Eq. 10b - 10k\{10c\}, Tab. 2, Tab. 4,}$$

$$\text{Kinetic model: (Eq. 1a - Eq. 2b) + (Eq. S.1 - Eq. S.2)} \tag{11}$$

As the decision for an SBR has already been made, the computationally expensive back-mixing parameter ξ no longer needs to be investigated and is hence fixed at 0 (see Table 4).

Table 4. Adjusted Variable Bounds for the Online Optimization of the Reductive Amination

decision variable	L.b.	U.b.	unit
j_i^{ext}	0		mol h^{-1}
T	358.15	383.15	K
p	10.0	25.0	bar
y_{H_2}	0.5	0.5	mol mol^{-1}
dT/dt	−600	600	K min^{-1}
dp/dt	0	0	bar min^{-1}
ξ	0.0	0.0	

Furthermore, the gas phase composition y_{H_2} is also fixed at 0.5 (Table 4), to ensure that the alcohol side reaction is always suppressed and comparability to previous studies[11] is improved. For a good comparison of the operation modes, the reaction time t_f is adjusted to the 6 h reaction residence time in the CSTR operation, although a high reaction activity can be observed for 8 h in the EPF optimization. As a conversion of more than 80% cannot be reached for the RA in 6 h under the chosen constraints, eq 10m is removed as a constraint. For comparability, the upper bounds for the decision variables pressure (p = 25 bar) and temperature (T110 °C) are also adjusted to the values used for the CSTR[11] operation, as shown in Table 4.

The pressure limit of 25 bar is also a technical limit of the settler sight-glass in the mini-plant. The change rate for the pressure is fixed at 0, as Table 4 shows. Thus, the optimizer can only choose the pressure for the full reaction time without changing it in between. This limitation is chosen to avoid foaming problems which can arise when dynamically lowering the pressure of an MES mixture.[10]

https://doi.org/10.1021/acs.iecr.4c02607
Ind. Eng. Chem. Res. 2025, 64, 520−534

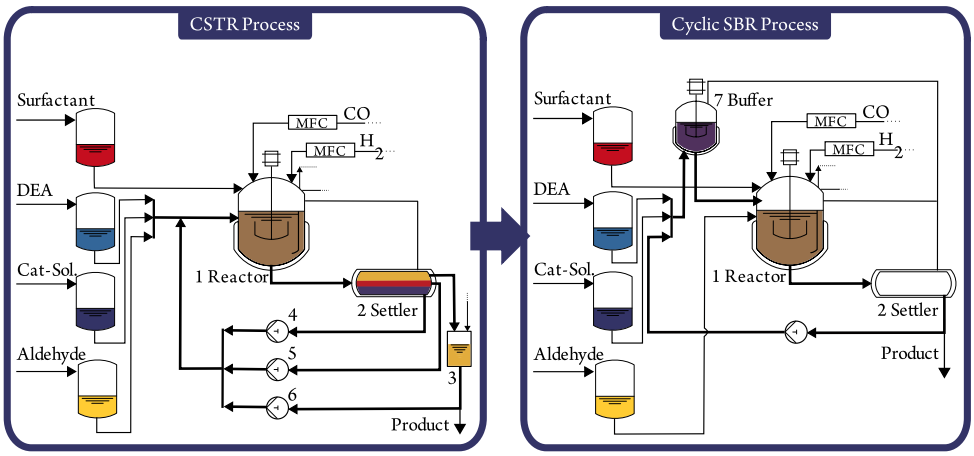

Figure 4. Mini-plant process adaptation from initial CSTR operation to cyclic semibatch operation.

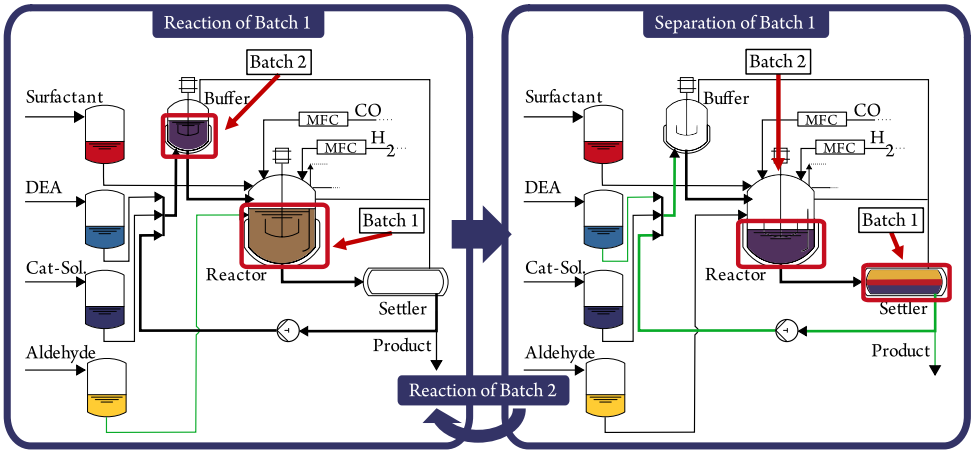

Figure 5. Cyclic semibatch operating concept.

In the online implementation of the EPF optimization, external dosing streams j_i^{ext} are only considered for the components DEA and aldehyde. As Figure 2 shows, only the dosing of enamine and aldol, which are formed in equilibrium reactions, could influence the reaction performance. DEUA and undecanol are formed in irreversible catalytic reactions and a dosage of these components would have a negative influence on the objective function as stated in eq 9. Water also takes part in the reaction but is already present in large amounts in MES. Further addition of the component would, hence, not influence the reaction. The consideration of an individual catalyst-, ligand-, or surfactant feed is not necessary during the mini-plant operation, since these components are supplied initially and fully recycled for the next reaction in the separation step.

With the adjusted EPF optimization problem, optimal control profiles can be predicted for each produced batch, as shown in Section 4.3. Due to adjusted starting values and constraints of a real mini-plant, the online EPF optimization leads to a different value for the optimal yield than eq 10 but still results in an SBR operation with the same dosing strategy as shown in Figure 3 and maxima for T = 110 °C and p = 25 bar.

4. IMPLEMENTATION AND VALIDATION OF AN OPTIMIZED REACTION TRAJECTORY IN A MINI-PLANT

In this section, an operation strategy for the optimized SBR operation a mini-plant is presented with details of the technical realization. Furthermore, the EPF optimization results are validated in a 125 h experimental mini-plant campaign and results are compared to other modes of operation.

4.1. Mini-Plant Process Design and Operating Strategy of Cyclic Semibatch Operation. This section is focused on developing an operating strategy for the cyclic SBR, which is an optimal match for the EPF trajectories (see Section 3.3) in combination with MES phase separation and catalyst recycling in a mini-plant. The transferal of the optimization result to a real mini-plant with the additional constraints introduced in the adapted online optimization (eq 11) is not assisted by further simulation. The operating strategy with integrated MES phase separation is developed based on results of the RA phase separation in MES[11] and similar SBR mini-plant implementations for the hydroformylation in TMS.[17−19] Here, one buffer tank before the SBR is required to store recycled catalyst solution and a second buffer tank after the SBR is needed for a steady feed into the continuous process.

For the current implementation of an optimal cyclic SBR operation with MES, an existing modular CSTR mini-plant[10,11,48] is modified, as shown in Figure 4.

https://doi.org/10.1021/acs.iecr.4c02607
Ind. Eng. Chem. Res. 2025, 64, 520−534

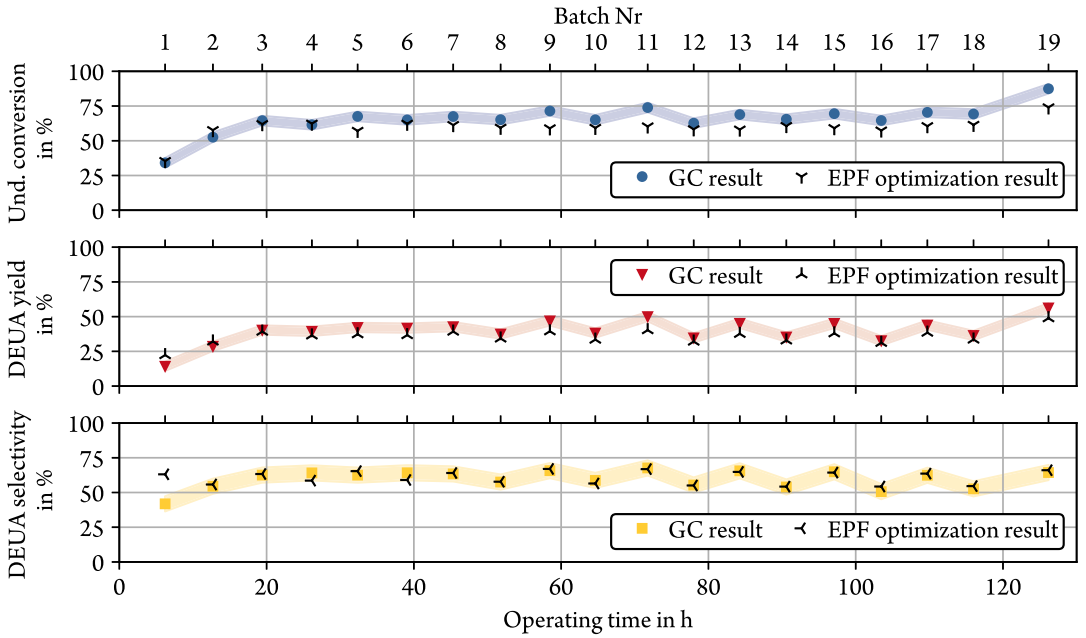

Figure 6. Reaction performance in the mini-plant during 125 h of cyclic semibatch operation compared to simulated EPF optimization results. Reaction conditions: 25 bar CO/H_2, τ_{SBR} = 6 h, 1200 rpm, T = 110 °C.

Instead of a continuous operation, we opted for a fully discontinuous operating strategy to benefit from a high operational flexibility, which is especially interesting concerning the challenging operation of the MES separation. The separation is not part of the EPF reactor optimization and its integration into the optimal cyclic SBR operation, as described in Section 3.3, is based on a previous phase separation investigation of the RA in MES.[11]

In the adaptation of the MES CSTR mini-plant shown in Figure 4, the settler (2) is used to separate the reaction mixture and functions as a buffer tank at the same time. This is a simplification compared to the TMS hydroformylation process[17−19] with two buffer tanks. The discontinuous settler operation also enables the removal of two pumps (5,6) and the oil buffer tank (3) of the CSTR setup in Figure 4. For the cyclic SBR implementation in the mini-plant, only one additional stirred buffer tank (7) for the recycled catalyst phase is required. If a continuously operated distillation column or membrane module is to be connected to the process for further product purification, an additional product buffer tank would be required.

Figure 5 shows the operating procedure of the cyclic SBR process design. The SBR process is operated with the mini-plant constraints (T = 110 °C, p = 25 bar, t_f = 6 h) which were introduced in Table 4 to enable comparison to previous mini-plant campaigns. During the reaction of the first batch, the educt aldehyde is continuously fed into the reactor. At the same time, a second mixture of catalyst-containing water phase, surfactant, and the diethylamine (DEA) educt is already present in the stirred buffer tank. Once the reaction of batch one is complete, the complete mixture is transferred to the settler within 5 min. When the reactor is completely empty, mixture 2 from the buffer tank is added to the reactor within 5 min. After a total downtime of 10 min, the next semibatch reaction starts. During the 6 h reaction residence time of batch two, the mixture of batch one can be separated in the settler. Once a phase separation is observed in the settler, the catalyst and surfactant-containing water phase are transferred back to the buffer tank, during which time the density at the outlet of the settler is monitored with a Coriolis flow sensor. A drop in the density is a clear sign that, instead of a mixture of surfactant and water (ρ > 1000 kg m^{-3} @80 °C), the product phase with a lower density (ρ < 800 kg m^{-3} @80 °C) is now leaving the settler. To ensure that no catalyst is lost, the first 5% of the oil phase are also transferred back to the buffer tank before the remaining oil phase is drawn from the process and collected in a product tank. Once the full water phase of batch one has reached the buffer tank, fresh diethylamine educt is added and the operating mode shown on the left in Figure 5 is restored. The next separation cycle begins as soon as the reaction of batch two is completed.

In addition to requiring two fewer pumps, the discontinuous operation of the settler has two major advantages. The first is the decoupling of the reaction and the separation step which have a strong influence on each other in the CSTR process and cause significant drawbacks in operability and stability of the overall process.[10,11,30] An independent separation and reaction step increases the operational flexibility and makes the plant more adaptable to load changes and potentially also to other reaction or component systems. The second advantage is a simplified separation step since no pumps need to be run at a rate proportionate to each of the liquid phases, which proved difficult in previous investigations.[10,11] The reacted mixture is filled into the settler and in a time window of 6 h until the next reaction batch is finished, the right separation temperature can be set and thermodynamic equilibrium in the separation step can always be ensured. This would allow for the settler to be built much smaller than in a CSTR process since an increase in residence time is no longer linked to an increase in vessel volume.

A further advantage of the discontinuous separation is that the reaction mixture of the RA can be separated in the two-phase region at lower temperatures instead of the three-phase region which is required in a CSTR process.[10,11,49] This way, the surfactant leaching can be reduced due to a lower surfactant concentration in the oil phase at lower temperatures.

https://doi.org/10.1021/acs.iecr.4c02607
Ind. Eng. Chem. Res. 2025, 64, 520−534

4.2. Process Equipment, Chemicals, and Analysis. The reductive amination in microemulsion systems in a 200 h CSTR mini-plant operation has already been reported in our previous contribution[11] with a detailed description of used equipment and analysis methods. The mini-plant process equipment from previous investigations[9−11,48] is adapted, and the same chemicals and analysis methods as for the CSTR RA investigation[11] are used. The catalyst solution is prepared under the exclusion of oxygen as outlined by Weber et al.[13]

The main experimental analytic results are based on GC measurements[11] (Agilent 7890A, HP-5 column 30 m × 320 μm × 0.25 μm, 5 wt % nonane IS) taken from the oil phase of each batch after separation in the settler. The rhodium content in the oil phase is determined from a representative sample of batch 6 with ICP-OES measurement.

The surfactant content in the oil phase of each batch is tracked through HPLC measurement[11] (Agilent 1260 HPLC with a C18 column [Kinetex 2.6 μm EVO, 100 Å, 100 × 4.6 mm]). The benzene ring in the surfactant Marlophen NP8 is detected in the HPLC with a variable length UV-detector at 225 nm.

As explained in Section 4.1, an additional 1.5 L stirred tank with a heating jacket is added to the plant setup. Pneumatic ball valves are introduced after each of the two stirred tanks and the settler for better operability of the discontinuous cyclic batch operation. For an accurate control of the surfactant content in the plant, a CETONI precision syringe pump is connected to the reactor. The surfactant content in the oil phase is measured with HPLC for each batch and the corresponding amount of surfactant lost in the oil phase is added back to the system before the start of the next reaction cycle. It is the first time that accurate surfactant tracking and dosing is used during a mini-plant investigation of MES. This is an important contribution toward better process controllability since the surfactant has a strong influence on reaction and separation performance.[4,49,50]

4.3. Experimental Results of a Cyclic Semibatch Mini-Plant Operation. Figure 6 shows the conversion, fatty amine yield, and selectivity of the 19 consecutive batches during the mini-plant operation. The displayed values are calculated from GC results that have an accuracy of ±1 wt % (see Section 4.2) and the resulting errors from Gaussian error propagation are X (±3.4 wt %), Y (±3.3 wt %) and S (±5.4 wt %). The performance for the even batches (2, 4, 6, etc.) in Figure 6 is generally slightly lower than that of the uneven batches. This is because the catalyst and surfactant content is lower in these batches while the amount of added educts is the same in all 19 batches. The ratio of undecanal educt to rhodium catalyst ($n_{\text{undecanal}}/n_{\text{Rh(acac)COD}}$) is 430 mol mol^{-1} for the uneven batches (1, 3, 5, etc.) and 625 mol mol^{-1} for the even batches. Consequently, fewer catalyst molecules are present in the even batches to produce the fatty amine, and the expected yield is lower. The performance of batches 1 and 19 deviates from the other batches. For batch 19, this is due to the extended reaction time of 9.8 h after an aldehyde dosing time of 6 h as in the other batches. For batch 1, the reduced performance is caused by an insufficient amount of the DEA educt provided at the start of the reaction, which was caused by a malfunctioning feed pump during plant startup.

In addition to the measured mini-plant results, Figure 6 also displays the optimization results predicted by the adapted EPF calculation in eq 11. An optimization is run for each batch with adjusted initial component hold-ups and feed rates, matching the values in the mini-plant. The corresponding start values and reaction times for each batch are shown in the Supporting Information in Tables S7−S9. The feed strategy remains the same throughout all optimized batches and the aldehyde dosing is always evenly distributed throughout the entire reaction time in a constant feed stream, as shown in Figure 3. Since the constraints, as set for the online optimization in eq 11, were not followed for batches 1 and 19 during the experimental validation, the optimizations were run with adjusted constraints. After adjusting the start value for DEA in batch 1 and the maximum reaction time in batch 19, the experimental results can be matched with the results of the adapted EPF optimization in eq 11, as Figure 6 shows.

The results in Figure 6 show that the developed kinetic model enables good prediction of the results obtained in a 125 h cyclic semibatch operation. For the selectivity shown in Figure 6, the predicted values only have an average deviation from the GC results of ±1.7 percentage points which is within the range of accuracy for the GC result (±5.4%). The predicted selectivity can thus be replicated perfectly in a mini-plant. For the conversion, the optimized EPF result is on average 6.8% lower than the mini-plant result. As a result of the lower prediction for the conversion, the predicted yield is also on average −4.2% lower than the GC results. The deviation of the conversion results from uncertainties in the kinetic model used in the EPF calculation where the reaction rate for the conversion of undecanal toward the intermediate enamine is underestimated (Figure S1 in Supporting Information). The kinetic model is the optimal fit for the currently available experimental data basis but still includes model uncertainties after parameter estimation. The resulting EPF optimum, hence, also includes a certain degree of uncertainty concerning the exact value of the conversion. An improved model with a reduction or quantification of the uncertainty would require additional kinetic experiments that show a stronger correlation between the varied process parameters and the enamine concentration. Despite the uncertainties, the optimization successfully leads to the identification of reaction trajectories which significantly improve the performance compared to a CSTR reference case, as Figures 3, 7, and 8 show.

When the composition of the oil phase at the end of a semibatch reaction is compared to that of a continuous CSTR operation,[11] a clear improvement in the plant performance becomes apparent, as Figure 7 shows. Given the same reaction conditions, the concentration of the educt in the SBR is on average 2.7 wt % lower than in the CSTR, indicating higher conversion. The concentration of the unwanted aldol side product is permanently lower than in the CSTR (on average 2 wt %), while the concentration of the target fatty amine component is considerably higher (4.7 wt %), indicating a higher selectivity. The reduced educt and side product concentrations in combination with a higher product concentration would also result in a reduced separation effort in a subsequent purification step toward pure fatty amine.

The increase in selectivity can also be seen in the experimental mini-plant results for different operating modes, shown in Figure 8. The figure further shows that the optimized cyclic SBR reactor concept from eq 10 and the subsequent online optimization of the reaction performance according to eq 11 successfully led to higher yields and selectivities compared to a standard batch operation or a CSTR[11] operation. This performance improvement was achieved despite the higher ratio of educt to catalyst molecules in the

https://doi.org/10.1021/acs.iecr.4c02607
Ind. Eng. Chem. Res. 2025, 64, 520−534

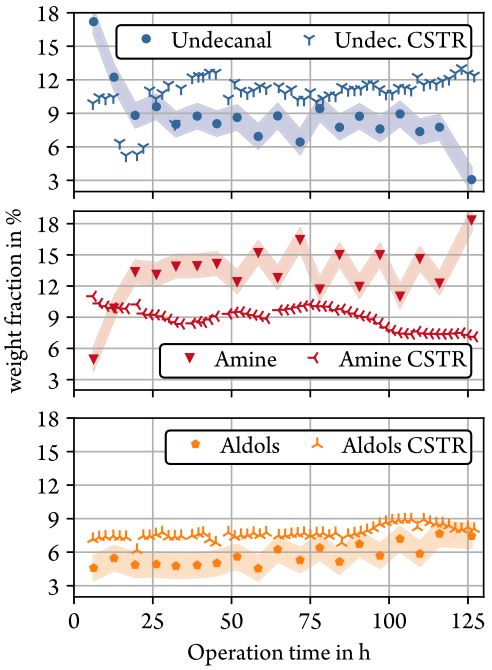

Figure 7. Weight fractions in cyclic SBR product stream compared to CSTR results (as shown in Duch et al.[11] between operating hour 56 and 177). SBR and CSTR were both operated at 110 °C, 25 bar, 1200 rpm. CSTR: $n_{undecanal}/n_{Rh(adac)COD}$ = 350 mol mol^{-1}. SBR (batch 1,3,5,etc.): $n_{undecanal}/n_{Rh(adac)COD}$ = 430 mol mol^{-1}. SBR (batch 2,4,6,etc.): $n_{undecanal}/n_{Rh(adac)COD}$ = 625 mol mol^{-1}.

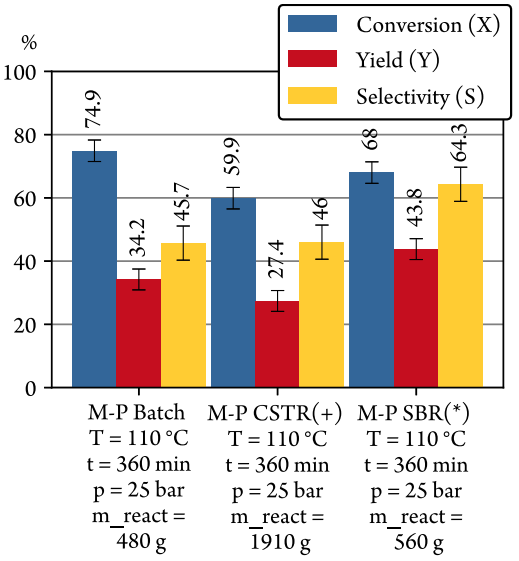

Figure 8. Comparison of reaction performance during mini-plant experiments for different modes of operation. +Values from Duch et al.[11] ($n_{undecanal}/n_{Rh(acac)COD}$ = 350). *Average of batch 3,5,7,9,11,13,15,17 ($n_{undecanal}/n_{Rh(acac)COD}$ = 430).

semibatch operation. The conversion in the semibatch is slightly lower than in the batch because the educt added at the end of the semibatch is still unreacted. Due to the high selectivity, the resulting product yield in the semibatch is still 9.6 percentage points higher than in the batch reaction and 16.4 percentage points higher than in the CSTR.

The combination of results in Figures 6−8 show that the optimized results of the EPF methodology have been successfully replicated in a mini-plant during a 125 h cyclic semibatch operation and that they lead to a considerable performance increase compared to a CSTR operation. This is an excellent showcase demonstrating the advantage of kinetic model development and model-based process synthesis to derive a process setup and operating strategy for micro-emulsion systems.

The performance improvement achieved in the current investigation by switching from a CSTR to a cyclic SBR operation is even more striking when looking at the fatty amine space-time yield (STY) in Figure 9. Optimization and

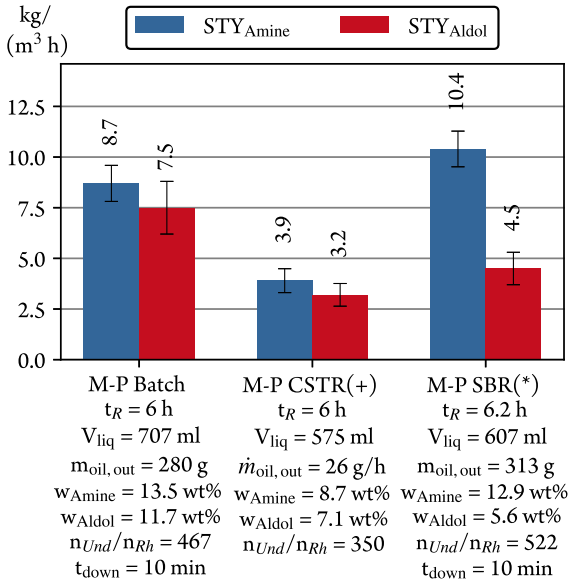

Figure 9. Comparison of fatty amine (DEUA) and aldol space-time yield for different modes of operation. Calculated with eq S3 of the Supporting Information. +Values from Duch et al.[11] *Average of batch 2−18.

experimental validation of the cyclic semibatch concept lead to a 266% increase of the amine STY (mass of product per liquid volume and reaction time, eq S3 in the Supporting Information) compared to the CSTR. The production capacity of the mini-plant is, thus, increased by the same factor just by changing the operating strategy. The batch operation in Figure 9 also has an amine STY almost as high as in the SBR, but the big advantage of the SBR is clearly shown by the significantly lower aldol STY. In the SBR, the largest amount of fatty amine is produced per time and volume while the ratio to the aldol side product formation is much lower than in the other operation modes.

Apart from the performance increase, the new operating strategy also has further advantages over a CSTR operation such as a simplified separation step which is decoupled from the reaction to increase operation flexibility as discussed in the introduction of the new mini-plant setup. The discontinuous separation in the SBR operation can be done at lower temperatures in the two-phase region. This separation state can not be selected for CSTR operation since the separation dynamic in this region is often slower than in the three-phase region (see Section 2.1).[31,49] In a discontinuous separation, the extended separation time is not an issue since up to 6 h (reaction time of the second batch) are available for separation. The reduced temperature in the two-phase region is desirable since, besides a lower energy requirement, it also results in a lower surfactant content in the oil phase.[11] The

https://doi.org/10.1021/acs.iecr.4c02607
Ind. Eng. Chem. Res. 2025, 64, 520−534

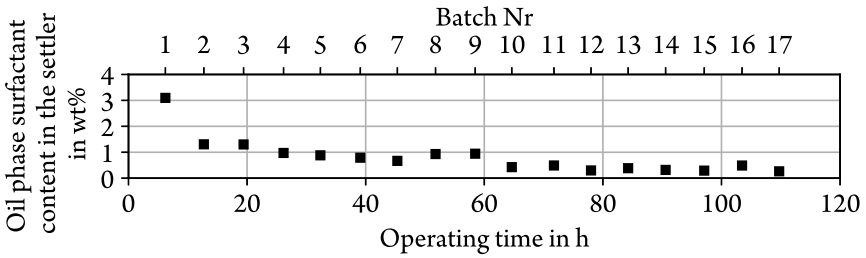

Figure 10. Oil phase surfactant concentration in the settler.

resulting low surfactant concentration can be seen in Figure 10. The results were obtained by HPLC measurement of the oil phase for each batch. The median of the surfactant concentration in the oil phase is 0.7 wt %. Therefore, 7.6 wt % of the surfactant entering the settler is lost when the oil phase leaves the process. A comparison of the surfactant loss with two-phase separation to the loss achieved in the previous three-phase CSTR operation[11] ($w_{\text{surf. in oil}}$ = 2.7 wt%, loss = 12.8 wt %) shows that the discontinuous operation of the settler can significantly improve surfactant retention.

To maintain the reaction performance, the equivalent amount of lost surfactant is added to the mixture at the start of the next batch cycle. This is the first time precise tracking and dosing of the surfactant was implemented in a mini-plant operation for microemulsion systems. As the constant reaction performance results in Figure 6 imply, the surfactant concentration in the reactor was successfully maintained.

Another point that is proven by the stable reaction performance over a period of 125 h in Figure 6, is the long-term catalyst stability. No additional catalyst was added to the initial mixtures during the entire operation in contrast to a previous investigation of the RA with MES in a CSTR process, where catalyst was added multiple times as a preventive measure.[11] The catalyst complexes thus remain stable in the reaction and separation step throughout the entire operation, in spite of also being stressed by temperature gradients and pumping in the cyclic operation. This is a promising result with regard to an industrial application where catalyst deterioration could be a significant cost factor. Besides the absence of catalyst degradation, the stable reaction performance also demonstrates the successful recovery of the catalyst in the separation step. In the oil outlet stream, a rhodium concentration of 2.2 mg kg^{-1} is measured. The resulting leaching rate, which is the ratio of the catalyst leaving the settler in the oil phase in relation to the catalyst entering the settler (as proposed by Kraume et al.[51]), is 0.92%. 99.08% of the catalyst are hence successfully recycled in an active form, which matches the result of the lab[13] and CSTR[11] operation. These results show that excellent catalyst recovery and long-term stability can be achieved in MES.

4.4. Applicability of Cyclic SBR Operation in Other MES Applications. The maximization of the reaction yield Y of the RA in MES as the product of conversion X and selectivity S ($Y = X \times S$) is the objective of the EPF optimization in the current study and can be achieved in an SBR. To evaluate ahead of further optimization calculations if the SBR concept can also achieve a maximum yield for other reactions in MES, selectivity and conversion need to be considered individually. The selectivity increase attainable in a semibatch operation compared to a CSTR is strongly dependent on the reaction network. In the current contribution, a reaction network with multiple noncatalytic equilibrium and side reactions is investigated, where selectivity has a strong influence on the product yield (Figure 2). As Figure 8 shows, the increased yield in the SBR operation compared to the CSTR is largely due to the increased selectivity, while the conversion is only slightly increased.

When considering the implementation of a cyclic SBR operation for the example of hydroformylation in MES, a significant increase in selectivity is not to be expected, as values of 92%[30] are already reached in a CSTR mini-plant operation. In the hydroformylation CSTR implementation, the conversion is the main limiting factor for a high yield and a cyclic SBR would not necessarily improve this. If, however, the hydroformylation is performed in a thermomorphic solvent system, EPF calculations for an optimal reactor concept with a cyclic SBR suggest a 24% selectivity increase.[17] The optimal process design and operating strategy derived with EPF optimization are strongly dependent on the specific reaction network and solvent system, and the EPF yields different results for each application. An EPF investigation to decide on a process setup and operating strategy for a given reaction and solvent system is hence always recommended. The cyclic semibatch operation leads to excellent results in the current investigation but is not generally the best mode of operation for all reactions in microemulsions. It is only the right choice if the main influence on the maximized plant yield is selectivity instead of conversion. The increased flexibility in a cyclic SBR operation, achieved by decoupling the reaction from the separation along with the simplified separation step, however, are factors that should also be considered for other reactions in microemulsion systems, even when a cyclic operation is not the first choice based on space-time yield.

5. CONCLUSIONS AND OUTLOOK

The EPF methodology is applied to the reductive amination of long-chain aldehydes in microemulsion systems to optimize the fatty amine yield. The dynamic optimization problem of the EPF methodology is constrained by a kinetic model of the RA in MES and yields optimal trajectories for the decsion variables: pressure, temperature, component dosing, back-mixing and gas-phase composition. The EPF trajectories can be approximated by a semibatch reactor, as an FPA reveals. The SBR should be operated cyclically to increase productivity. An existing mini-plant is adapted to incorporate this new process design and operating strategy. The EPF optimization reveals an increase in conversion, yield, and selectivity for a cyclic SBR operation compared to a previous CSTR operation. These optimization results can also be validated in a 125 h mini-plant operation, demonstrating an excellent transfer from simulation to experiment. The fatty amine yield achieved in the mini-plant with a cyclic SBR operation is 16.4 percentage

https://doi.org/10.1021/acs.iecr.4c02607
Ind. Eng. Chem. Res. 2025, 64, 520−534

points higher than in a comparable CSTR operation and the STY is increased by 266%. This is an excellent demonstration of the large performance increase achievable by using EPF optimization to select a process design and operating strategy, and it further demonstrates the operational versatility and process maturity of reactions in MES. The goal of maximization of the amine yield was achieved despite uncertainties in the underlying kinetic model. In the future, an extension of the experimental data basis which allows the quantification of the model uncertainty would enable a more accurate optimization under uncertainties.

The discontinuous cyclic operation in the redesigned process does not require additional process equipment compared to a CSTR operation. Instead, the setup can be simplified by removing two pumps. The discontinuous operation of the settler makes the separation step easier to control and allows for a separation in the two-phase region that usually has a longer separation time but also a more favorable low surfactant content in the oil phase. The increased flexibility of a discontinuous SBR operation is usually outweighed by the higher productivity of a CSTR. This is not the case for the current application of a cyclic SBR for the reductive amination.

In the current mini-plant operation, accurate surfactant tracking and dosing are implemented for the first time, leading to excellent process controllability and a very stable reaction performance. The constant performance is also only achievable through excellent catalyst recycling. 99.1% of the catalyst entering the settler is recycled in active form after each batch, ensuring constant performance without any catalyst addition during a 125 h operation. This excellent catalyst retention and long-term stability demonstrate once again the large potential of microemulsion systems as a reaction concept for homogeneous catalysis.

A further process improvement with respect to sustainability and productivity could be achieved through the reduction or omittance of the organic cosolvent dodecane. Usually, MES are an option to replace organic cosolvents in synthesis, and the reductive amination only requires dodecane to reduce the educt aldehyde concentration and limit the side reaction toward aldols. A switch to semibatch operation with aldehyde dosing follows the same logic and further investigations should be conducted for the RA in an SBR without dodecane cosolvent. The reduction of cosolvent also directly influences the space-time yield as more product per volume can be produced. Under this aspect, the oil-to-water ratio α of MES should also be reinvestigated and optimized. A water content of 50 wt % is chosen in most MES investigations to benefit from a large phase separation temperature region and interfacial area for the catalytic reaction to take place. But for economic industrial production, the optimal value might be lower.

A further possibility to limit the aldol formation is the combination of the hydroformylation with the RA in the hydroaminomethylation tandem reaction. In the HAM, the hydroformylation aldehyde production is slower than the subsequent reductive amination. This strongly limits the aldehyde concentration and the corresponding aldol formation and, thus, results in excellent amine selectivity.[52] An EPF investigation for the HAM in TMS[32] shows promising results and the next step would be to also apply the EPF methodology to HAM in MES and verify the results experimentally.

■ ASSOCIATED CONTENT

Supporting Information

The Supporting Information is available free of charge at https://pubs.acs.org/doi/10.1021/acs.iecr.4c02607.

Additional kinetic equations, model parameters, initial component hold-ups for each batch, and an exemplary plot for the parameter estimation are provided in the Supporting Information (PDF)

■ AUTHOR INFORMATION

Corresponding Author

Karsten Duch − *Process Dynamics and Operations Group, Technische Universität Berlin, Berlin D-10623, Germany;* orcid.org/0009-0002-5308-2700; Email: karsten.duch@tu-berlin.de

Authors

Volodymyr Kozachynskyi − *Process Dynamics and Operations Group, Technische Universität Berlin, Berlin D-10623, Germany;* orcid.org/0000-0001-9607-4298

Karsten H. G. Rätze − *Chair for Process Systems Engineering, Otto von Guericke University Magdeburg, Magdeburg D-39106, Germany;* orcid.org/0000-0001-5337-8566

Markus Illner − *Process Dynamics and Operations Group, Technische Universität Berlin, Berlin D-10623, Germany;* orcid.org/0000-0003-1500-9588

Kai Sundmacher − *Chair for Process Systems Engineering, Otto von Guericke University Magdeburg, Magdeburg D-39106, Germany; Department Process Systems Engineering, Max Planck Institute for Dynamics of Complex Technical Systems, Magdeburg D-39106, Germany;* orcid.org/0009-0008-8156-0611

Jens-Uwe Repke − *Process Dynamics and Operations Group, Technische Universität Berlin, Berlin D-10623, Germany*

Complete contact information is available at: https://pubs.acs.org/10.1021/acs.iecr.4c02607

Notes

The authors declare no competing financial interest.

■ ACKNOWLEDGMENTS

Gefördert durch die Deutsche Forschungsgemeinschaft (DFG) - TRR 63 “Integrierte chemische Prozesse in flüssigen Mehrphasensystemen” (Teilprojekt B1, D2, D4) - 56091768. This work is funded by the Deutsche Forschungsgemeinschaft (DFG, German Research Foundation) - TRR 63 “Integrated Chemical Processes in Liquid Multiphase Systems” (subprojects B1, D2, D4) - 56091768. Financial support is gratefully acknowledged. Furthermore, the authors gratefully acknowledge the support of Umicore N.V. for sponsoring the rhodium catalyst precursor “acetylacetonato(1,5-cyclooctadiene)rhodium(I) (CAS Registry Number 12245-39-5)”, Sasol Ltd. for the surfactant used in the described experiments, the support of SIEMENS AG for sponsoring the entire process control system SIMATIC PCS7 for the automation of the mini-plant. The authors would also like to thank Hannes Raddant (TU Berlin) for the support in the development of the HPLC surfactant tracking method and Lorenz Hafner (TU Berlin) for the support with the adaptation of the kinetic equitation system.

NOMENCLATURE

Abbreviations

AR	attainable region
BR	batch reactor
CSTR	continuously stirred tank reactor
DEA	diethylamine
DEUA	diethylundecylamine
DOP	dynamic optimization problem
DSR	distributed side-stream reactor
EPF	elementary process function
FPA	flux profile analysis
GC	gas chromatography
HAM	hydroaminomethylation
HPLC	high-performance liquid chromatography
ICP-OES	Inductively Coupled Plasma − Optical Emission Spectroscopy
MES	microemulsion system(s)
PFTR	plug flow tube reactor
RA	reductive amination
SBR	semibatch reactor
STY	space time yield
TMS	thermomorphic solvent system(s)

Symbols

K	equilibrium constant
k	pre-exponential factor
p	pressure
$\mathcal{RCT}$	reactions (eq [1a]−[1d])
$\mathcal{SPC}$	component species (Table [1])
T	temperature

Subscripts

Amine	amine
Aldols	aldols
cat	catalyst
DEA	diethylamine
En	enamine
EQa	equilibrium reaction a
EQb	equilibrium reaction b
ext	external dosing
f	final time
H_2	hydrogen
H_2O	water
HYDa	catalytic hydration reaction a
HYDb	catalytic hydration reaction b
i	component species index ($\mathcal{SPC}$, Table [1])
j	reaction index ($\mathcal{RCT}$, eq [1a]−[1d])
k	equilibrium reaction index ({EQa, EQb})
m	amine and enamine intermediate
ligand	ligand
Liq	liquid
nC11al	undecanal (aldehyde)
nC12an	dodecane (cosolvent)
oil	oil
ST	storage tank
sub	substrate
surf	surfactant

Superscripts

ext	external
max	maximum
opt	optimal
sat	saturation
ST	storage tank

REFERENCES

(1) Lipshutz, B. H.; Ghorai, S. Transitioning organic synthesis from organic solvents to water. What's your E Factor? *Green Chem.* **2014**, *16*, 3660−3679.

(2) La Sorella, G.; Strukul, G.; Scarso, A. Recent advances in catalysis in micellar media. *Green Chem.* **2015**, *17*, 644−683.

(3) Schwarze, M.; Pogrzeba, T.; Volovych, I.; Schomäcker, R. Microemulsion systems for catalytic reactions and processes. *Catalysis Science and Technology* **2015**, *5*, 24−33.

(4) Fabris, F.; Illner, M.; Repke, J.-U.; Scarso, A.; Schwarze, M. Is Micellar Catalysis Green Chemistry? *Molecules (Basel, Switzerland)* **2023**, *28*, 4809.

(5) Hamerla, T.; Rost, A.; Kasaka, Y.; Schomäcker, R. Hydroformylation of 1−Dodecene with Water−Soluble Rhodium Catalysts with Bidentate Ligands in Multiphase Systems. *ChemCatChem.* **2013**, *5*, 1854−1862.

(6) Kraume, M.; Enders, S.; Drews, A.; Schomäcker, R.; Engell, S.; Sundmacher, K., Eds. *Integrated Chemical Processes in Liquid Multiphase Systems: From chemical reaction to process design and operation*, 1st ed.; De Gruyter: Berlin, 2022; p. 32.

(7) Schwuger, M.-J.; Stickdorn, K.; Schomaecker, R. Microemulsions in Technical Processes. *Chem. Rev.* **1995**, *95*, 849−864.

(8) Kraume, M.; Enders, S.; Drews, A.; Schomäcker, R.; Engell, S.; Sundmacher, K., Eds. *Integrated Chemical Processes in Liquid Multiphase Systems: From chemical reaction to process design and operation*, 1st ed.; De Gruyter: Berlin, 2022; p. 1.

(9) Pogrzeba, T.; Müller, D.; Hamerla, T.; Esche, E.; Paul, N.; Wozny, G.; Schomäcker, R. Rhodium-Catalyzed Hydroformylation of Long-Chain Olefins in Aqueous Multiphase Systems in a Continuously Operated Miniplant. *Ind. Eng. Chem. Res.* **2015**, *54*, 11953−11960.

(10) Illner, M.; Müller, D.; Esche, E.; Pogrzeba, T.; Schmidt, M.; Schomäcker, R.; Wozny, G.; Repke, J. U.; Repke, J.-U. Hydroformylation in Microemulsions: Proof of Concept in a Miniplant. *Ind. Eng. Chem. Res.* **2016**, *55*, 8616−8626.

(11) Duch, K.; Kozachynskyi, V.; Porthun, L.; Illner, M.; Repke, J.-U. Continuous Homogeneously Catalyzed Production of Fatty Amines in Microemulsions - Proof of Concept in a Mini-Plant. *Ind. Eng. Chem. Res.* **2024**, *63*, 8916−8932.

(12) Kirschtowski, S.; Kadar, C.; Seidel-Morgenstern, A.; Hamel, C. Kinetic Modeling of Rhodium−Catalyzed Reductive Amination of Undecanal in Different Solvent Systems. *Chem.-Ing.-Technol.* **2020**, *92*, 582−588.

(13) Weber, A.; Porthun, L.; Schomäcker, R. Rh-Catalyzed Reductive Amination of Undecanal in an Aqueous Microemulsion System Using a Non-Ionic Surfactant. *Catalysts* **2021**, *11*, 1223.

(14) Freund, H.; Sundmacher, K. Towards a methodology for the systematic analysis and design of efficient chemical processes. *Chemical Engineering and Processing: Process Intensification* **2008**, *47*, 2051−2060.

(15) Peschel, A.; Freund, H.; Sundmacher, K. Methodology for the Design of Optimal Chemical Reactors Based on the Concept of Elementary Process Functions. *Ind. Eng. Chem. Res.* **2010**, *49*, 10535−10548.

(16) Hentschel, B.; Peschel, A.; Freund, H.; Sundmacher, K. Simultaneous design of the optimal reaction and process concept for multiphase systems. *Chem. Eng. Sci.* **2014**, *115*, 69−87.

(17) Kaiser, N. M.; Jokiel, M.; McBride, K.; Flassig, R. J.; Sundmacher, K. Optimal Reactor Design via Flux Profile Analysis for an Integrated Hydroformylation Process. *Ind. Eng. Chem. Res.* **2017**, *56*, 11507−11518.

(18) Rätze, K. H.; Jokiel, M.; Kaiser, N. M.; Sundmacher, K. Cyclic operation of a semi-batch reactor for the hydroformylation of long-chain olefins and integration in a continuous production process. *Chemical Engineering Journal* **2019**, *377*, 120453.

(19) Jokiel, M.; Rätze, K. H. G.; Kaiser, N. M.; Künnemann, K. U.; Hollenbeck, J.-P.; Dreimann, J. M.; Vogt, D.; Sundmacher, K. Miniplant-Scale Evaluation of a Semibatch-Continuous Tandem

https://doi.org/10.1021/acs.iecr.4c02607
Ind. Eng. Chem. Res. 2025, 64, 520−534

Reactor System for the Hydroformylation of Long-Chain Olefins. *Ind. Eng. Chem. Res.* **2019**, *58*, 2471−2480.
(20) Kaiser, N. M.; Flassig, R. J.; Sundmacher, K. Reactor-network synthesis via flux profile analysis. *Chemical Engineering Journal* **2018**, *335*, 1018−1030.
(21) Brunsch, Y.; Behr, A. Temperature-controlled catalyst recycling in homogeneous transition-metal catalysis: minimization of catalyst leaching. *Angewandte Chemie (International ed. in English)* **2013**, *52*, 1586−1589.
(22) Gaide, T.; Dreimann, J. M.; Behr, A.; Vorholt, A. J. Overcoming Phase-Transfer Limitations in the Conversion of Lipophilic Oleo Compounds in Aqueous Media-A Thermomorphic Approach. *Angew. Chem. Int. Ed.* **2016**, *55*, 2924−2928.
(23) Bianga, J.; Künnemann, K. U.; Gaide, T.; Vorholt, A. J.; Seidensticker, T.; Dreimann, J. M.; Vogt, D. Thermomorphic Multiphase Systems: Switchable Solvent Mixtures for the Recovery of Homogeneous Catalysts in Batch and Flow Processes. *Chem.—Eur. J.* **2019**, *25*, 11586−11608.
(24) Behr, A.; Henze, G.; Schomäcker, R. Thermoregulated Liquid/Liquid Catalyst Separation and Recycling. *Advanced Synthesis & Catalysis* **2006**, *348*, 1485−1495.
(25) Kraume, M.; Enders, S.; Drews, A.; Schomäcker, R.; Engell, S.; Sundmacher, K., Eds. *Integrated Chemical Processes in Liquid Multiphase Systems: From chemical reaction to process design and operation*, 1st ed.; De Gruyter: Berlin, 2022.
(26) Kraume, M.; Enders, S.; Drews, A.; Schomäcker, R.; Engell, S.; Sundmacher, K., Eds. *Integrated Chemical Processes in Liquid Multiphase Systems: From chemical reaction to process design and operation*, 1st ed.; De Gruyter: Berlin, 2022; p. 63.
(27) Kahlweit, M.; Strey, R.; Firman, P.; Hasse, D.; Jen, J.; Schomäcker, R. General Patterns of the Phase Behavior of Mixtures of H2O, Nonpolar Solvents, Amphiphiles, and Electrolytes. 1 // General Patterns. *Langmuir* **1988**, *4*, 499−511.
(28) Sottmann, T.; Stubenrauch, C. *Microemulsions*; Stubenrauch, C., Ed.; John Wiley & Sons, Ltd: Chichester, UK, 2009; pp. 1−47.
(29) Schwarze, M.; Pogrzeba, T.; Seifert, K.; Hamerla, T.; Schomäcker, R. Recent developments in hydrogenation and hydroformylation in surfactant systems. *Catal. Today* **2015**, *247*, 55−63.
(30) Illner, M.; Kozachynskyi, V.; Esche, E.; Repke, J.-U. Fast-track realization of reactive microemulsion systems−Systematic system analysis and tailored application of PSE methods. *Chem. Eng. Sci.* **2022**, *252*, No. 117290.
(31) Kasaka, Y.; Bibouche, B.; Volovych, I.; Schwarze, M.; Schomäcker, R. Investigation of phase behaviour of selected chemical reaction mixtures in microemulsions for technical applications. *Colloids Surf., A* **2016**, *494*, 49−58.
(32) Rätze, K. H. G. Computer-aided model development, process design and operating strategies for transient liquid multiphase systems. Ph.D. thesis, Otto-von-Guericke-Universität Magdeburg: Magdeburg, 2023.
(33) Chen, Q.; Grossmann, I. E. Recent Developments and Challenges in Optimization-Based Process Synthesis. *Annu. Rev. Chem. Biomol. Eng.* **2017**, *8*, 249−283.
(34) Kaiser, S.; Engell, S. An integrated approach to fast model-based process design: Integrating superstructure optimization under uncertainties and optimal design of experiments. *Chem. Eng. Sci.* **2023**, *269*, No. 118453.
(35) Weigert, J.; Illner, M.; Esche, E.; Repke, J.-U. Development of a State Estimation Environment for the Optimal Control of a Miniplant for the Hydroformylation in Microemulsions. *Chem. Eng. Trans.* **2018**, *70*, 973−978.
(36) Müller, D.; Illner, M.; Esche, E.; Pogrzeba, T.; Schmidt, M.; Schomäcker, R.; Biegler, L. T.; Wozny, G.; Repke, J. U.; Repke, J.-U. Dynamic real-time optimization under uncertainty of a hydroformylation mini-plant. *Comput. Chem. Eng.* **2017**, *106*, 836−848.
(37) Illner, M.; Kozachynskyi, V.; Esche, E.; Repke, J.-U. *14th International Symposium on Process Systems Engineering*; Computer Aided Chemical Engineering; Elsevier, 2022; Vol. *49*; pp. 433−438.
(38) Kirschtowski, S.; Jameel, F.; Stein, M.; Seidel-Morgenstern, A.; Hamel, C. Kinetics of the reductive amination of 1-undecanal in thermomorphic multicomponent system. *Chem. Eng. Sci.* **2021**, *230*, No. 116187.
(39) Pogrzeba, T.; Illner, M.; Schmidt, M.; Milojevic, N.; Esche, E.; Repke, J. U.; Schomäcker, R.; Repke, J.-U. Kinetics of Hydroformylation of 1-Dodecene in Microemulsion Systems Using a Rhodium Sulfoxantphos Catalyst. *Ind. Eng. Chem. Res.* **2019**, *58*, 4443−4453.
(40) Bianga, J.; Künnemann, K. U.; Goclik, L.; Schurm, L.; Vogt, D.; Seidensticker, T. Tandem Catalytic Amine Synthesis from Alkenes in Continuous Flow Enabled by Integrated Catalyst Recycling. *ACS Catal.* **2020**, *10*, 6463−6472.
(41) Kozachynskyi, V.; Illner, M.; Esche, E.; Repke, J.-U. The optimal experiment? Influence of solution strategies on model-based optimal experimental design. *Comput. Chem. Eng.* **2024**, *187*, No. 108746.
(42) Wunderlich, J.; Kretzschmar, P.; Schomäcker, R. Integrated techno-economic and life cycle assessment of hydroformylation in microemulsion systems. *Front. Sustain.* **2024**, *5*, No. 1405471.
(43) Biegler, L. T., Ed. *Nonlinear Programming: Concepts, algorithms, and applications to chemical processes*; MOS-SIAM series on optimization; Society for Industrial and Applied Mathematics: Philadelphia, PA, 2010; Vol. *10*; p. 271.
(44) Wächter, A.; Biegler, L. T. On the implementation of an interior-point filter line-search algorithm for large-scale nonlinear programming. *Mathematical Programming* **2006**, *106*, 25−57.
(45) Science and Technology Facilites Council. *The HSL Mathematical Software Library*. https://www.hsl.rl.ac.uk/.
(46) Andersson, J. A. E.; Gillis, J.; Horn, G.; Rawlings, J. B.; Diehl, M. CasADi: a software framework for nonlinear optimization and optimal control. *Mathematical Programming Computation* **2019**, *11*, 1−36.
(47) Jokiel, M.; Kaiser, N. M.; Kováts, P.; Mansour, M.; Zähringer, K.; Nigam, K. D. P.; Sundmacher, K. Helically coiled segmented flow tubular reactor for the hydroformylation of long-chain olefins in a thermomorphic multiphase system. *Chemical Engineering Journal* **2019**, *377*, 120060.
(48) Müller, M.; Kasaka, Y.; Müller, D.; Schomäcker, R.; Wozny, G. Process Design for the Separation of Three Liquid Phases for a Continuous Hydroformylation Process in a Miniplant Scale. *Ind. Eng. Chem. Res.* **2013**, *52*, 7259−7264.
(49) Müller, D.; Esche, E.; Pogrzeba, T.; Illner, M.; Leube, F.; Schomäcker, R.; Wozny, G. Systematic Phase Separation Analysis of Surfactant-Containing Systems for Multiphase Settler Design. *Ind. Eng. Chem. Res.* **2015**, *54*, 3205−3217.
(50) Pogrzeba, T.; Schmidt, M.; Milojevic, N.; Urban, C.; Illner, M.; Repke, J. U.; Schomäcker, R.; Repke, J.-U. Understanding the Role of Nonionic Surfactants during Catalysis in Microemulsion Systems on the Example of Rhodium-Catalyzed Hydroformylation. *Ind. Eng. Chem. Res.* **2017**, *56*, 9934−9941.
(51) Kraume, M.; Enders, S.; Drews, A.; Schomäcker, R.; Engell, S.; Sundmacher, K., Eds. *Integrated Chemical Processes in Liquid Multiphase Systems: From chemical reaction to process design and operation*, 1st ed.; De Gruyter: Berlin, 2022; p. 47.
(52) Weber, A.; Porthun, L.; Schomäcker, R. One-Pot Synthesis of Fatty Amines: Rh-Catalyzed Hydroaminomethylation of 1-Decene in an Aqueous Microemulsion System—Influence of Reaction Conditions on the Reaction Performance. *Catalysts* **2022**, *12*, 773.

https://doi.org/10.1021/acs.iecr.4c02607
Ind. Eng. Chem. Res. 2025, 64, 520−534